A novel high-throughput FLIPR Tetra based method for capturing highly confluent kinetic data for structure-kinetic relationship guided early drug discovery

Puneet Khurana[#,1], Lisa McWilliams[#,1], Jonathan Wingfield[#], Derek Barratt[#], Bharath Srinivasan[#, 2]

[#] Mechanistic Biology and Profiling, Discovery Sciences, R&D, AstraZeneca, Cambridge, UK

[1]These authors contributed equally to this work

[2]Corresponding author, bharath.srinivasan@astrazeneca.com, +447508382559

Graphical abstract:

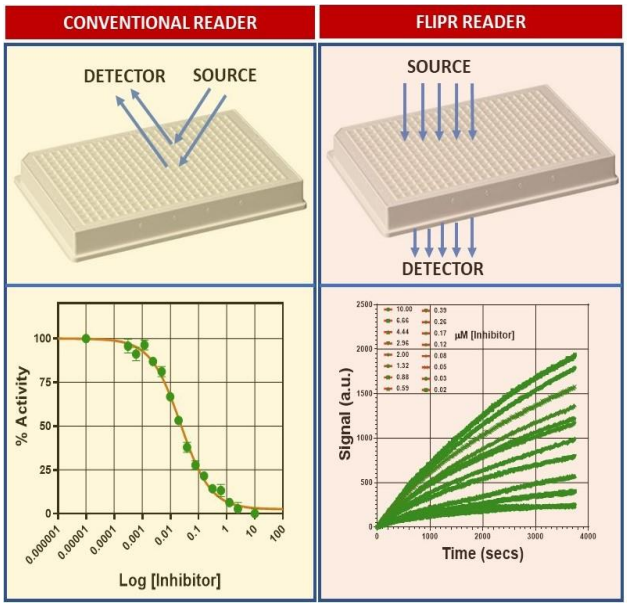

Keywords: *Kinetics, progress curve analysis, FLIPR Tetra, high-throughput screening, covalent inhibition, slow onset inhibition, association rate, dissociation rate, structure-kinetic relationship*

Abbreviations: *SKR, structure-kinetic relationship; BK, binding kinetics; LI, Lead Identification; HTS, high-throughput screening; FLIPR, Fluorescent Imaging Plate Reader; MoA, Mechanism of Action; SAR, structure-activity relationship; DMSO, dimethyl sulfoxide, DRC, dose response curve; FI, Fluorescence intensity; CHEF, chelation enhanced fluorescence; CCD, charge-coupled device.*

Abstract:

Target engagement by small-molecules is necessary for producing a physiological outcome. In the past, a lot of emphasis was placed on understanding the thermodynamics of such interactions to guide structure-activity relationship. However, it is becoming clearer that understanding the kinetics of the interaction between a small molecule inhibitor and the biological target (structure kinetic relationship, SKR) is critical for selection of the optimum candidate drug molecule for clinical trial. However, the acquisition of kinetic data in high-throughput manner using traditional methods can be labor intensive, limiting the number of molecules that can be tested. As a result, in depth kinetic studies are often carried out only on a small number of compounds and, usually, at a later stage in the drug discovery process. Fundamentally, kinetic data should be used to drive key decisions much earlier in the drug discovery process but the throughput limitations of traditional methods precludes this. A major limitation that hampers acquisition of high-throughput kinetic data is the technical challenge in collecting substantially confluent datapoints for

accurate parameter estimation from time-course analysis. Here we describe the use of Fluorescent Imaging Plate Reader (FLIPR), a CCD camera technology, as a potential high-throughput tool for generating biochemical kinetic data with smaller time-intervals. Subsequent to the design and optimization of the assay, we demonstrate the collection of highly confluent time-course data for various kinase protein targets with reasonable throughput to enable SKR-guided medicinal chemistry. We select kinase target 1 as a special case study with covalent inhibition and demonstrate methods for rapid and detailed analysis of the resultant kinetic data for parameter estimation . In conclusion, this approach has the potential to enable rapid kinetic studies to be carried out on 100's of compounds per week and drive project decisions with kinetic data at an early stage in drug discovery.

1.1. Introduction

The importance of understanding binding kinetics (BK) of compounds in early stages of drug discovery has been well recognized over the last decade[1–3]. Traditional approaches to use steady-state affinity for triaging compounds at the lead identification (LI) stage use binding thermodynamics as a guide in their structure-activity relationship (SAR) guided small-molecule synthesis. However, this approach is proving inadequate without involving structure-kinetic relationship (SKR)[4]. This is because binding thermodynamics assumes equilibrium conditions which is rarely the case in physiological drug-target interaction. Increasing number of studies are showing how the absolute magnitudes of the second-order association rate constant (k_{on})[5], first-order dissociation rate constant (k_{off}) and residence time ($1/k_{off}$), indicating the lifetime of drug-target complex, are dictating real physiological outcomes rather than ratiometric equilibrium constants[6–12]. This becomes all the more pertinent in open-systems, as is the case with the human organism, where several competing factors like pharmacokinetics, pharmacodynamics, target half-life and so forth convolute the landscape of drug-target interactions[13–18]. Furthermore, projects optimizing for covalent inhibitors have been wrongly employing a time-, affinity- and substrate concentration-dependent parameter like IC_{50} as a metric to drive SAR[19]. The ideal parameter to estimate for covalent inhibition would be the second order rate constant k_{inact}/K_I given the time-dependent potency gain displayed by this class of inhibitors[19]. A typical affinity-based project cascade that is potency driven can underestimate a chemical series with poor affinity but desirable binding kinetics (BK) for the target of interest. This can undermine effective LI by ignoring compound series that, upon medicinal chemistry intervention, could have delivered both desirable BK and potency. It should be noted that compounds with similar functional activity could have dissimilar BK profile[15,20]. Though binding kinetics under turnover conditions is often ignored during the early phase in a typical drug discovery pipeline, acquiring and employing this information in early drug discovery can potentially contribute towards decreasing the attrition rate at a later date[15].

Assay technologies and advanced data analysis tools are available for running biochemical kinetic assays. However, the pharmaceutical industry is still struggling with capturing biochemical kinetic data in a high-throughput fashion. Biochemical kinetic characterization of inhibitors requires quantitative measures of enzyme activity at very short-time intervals to capture the time-dependence of the reaction rate. Since standard photo-multiplier tube (PMT) based plate readers read one well at a time, the time interval for reading a full 384 plate is approximately 1.5 mins which is unacceptably long if the experiment requires

estimation of time-dependent rates of initial reaction (<5% substrate to product conversion) for reactions with reasonable k_{cat} values (turnover in minutes). Furthermore, the resolution of the initial rate representing the first couple of turnovers would be highly valuable in estimating pre-steady state parameters that shed critical insights into the chemical events happening at the active site. This can only be achieved with greater confluence of data points at those initial time-points that cannot be generated with current plate-based readers. Covalent and slow-onset inhibitors showing non-linear progress curves with distinct initial velocity ($v°$) and steady state velocity (v^{ss}) phases are yet another example where confluent data points will aid in capturing the transition from initial to steady state phase accurately and, in turn, help estimate kinetic parameters with greater accuracy. Lack of points at the zone of transition (from $v°$ to v^{ss}) will hamper the precise estimation of k_{obs} and, thus, $k_{on}{}^{app}$ and k_{off} subsequently. It will also result in inaccurate estimates for the second order parameter k_{inact}/K_I. Therefore, laser-based plate readers are limited to low-throughput biochemical kinetic studies.

In a typical SAR led program, high-throughput screening (HTS) is deployed to identify compounds for subsequent IC_{50} studies. In a similar way, there is a need for first-pass high-throughput mechanistic characterization for large number of compounds to triage compounds for further detailed mechanistic characterization at low-throughput. Using several representative kinase protein targets, we have delivered a novel application of FLIPR to generate high quality biochemical kinetic data achieving better confluence than laser-based readers, meeting the demands of mechanistic characterization at the lead identification (LI) stage. In our examples, AssayQuant technology employing Chelation-Enhanced Fluorescence (ChEF) by a Sox-containing peptide was used for assaying protein kinase activity allowing real time monitoring of kinase activity.[21–24]. Progress curve analysis was performed using the Genedata Mechanistic analysis package which facilitated delivery of a high-throughput system by reducing analysis time.

This study, to the best of our knowledge, is the first to demonstrate the use of FLIPR for generating high-throughput biochemical kinetic data in a target agnostic manner at an early stage in the drug discovery process. Further, it demonstrates the importance of collecting confluent data points for precise parameter estimation in an early stage drug discovery process to enable highly reliable SKR guided medicinal chemistry.

1.2. Material and Methods

1.2.1. Compound handling

Known covalent inhibitors of the different kinase targets (kinase 1, kinase 2, kinase 3 and kinase 4) were selected from the AZ compound collection. Assay ready compound plates (ARP) were prepared by acoustically dispensing 18 chosen compounds into a 384-well black, clear bottomed microtiter plate (Corning 3544). A range of different volumes were dispensed to create 16 point concentration response curves, 1:1.5 dilution with a final compound concentration range between 10 µM and 22 nM. All wells were backfilled with the appropriate volume of DMSO to achieve a final concentration of 1 % v/v DMSO in a 10 µl final assay volume. All ARPs included neutral controls (no inhibition, 1 % v/v DMSO) and inhibitor controls (100 % inhibition, 20 µM of assay-specific compound) to determine the linearity window of the assay.

1.2.3. Biochemical kinetic assay

AssayQuant technology was used to allow real time monitoring of kinase activity in a continuous and homogenous assay format. The biochemical assay measured increase in

chelation enhanced fluorescence (CHEF) for quantifying real-time phosphorylation of the sox peptide, as a measure of kinetic activity[21–24]. Working stocks of protein (kinase 1) and substrate mix (AQT-099 + ATP) were prepared in assay buffer (20 mM HEPES pH 7.5, 0.005% BRIJ-35, 0.5 mg/ml BSA, 5 mM $MgCl_2$, 5% glycerol). 5 µl/well of substrate mix was dispensed followed by 5 µl/well of protein mix into ARP using Certus FLEX, a liquid dispenser. The plate was immediately sealed (BIO-RAD Catalogue no: MSB1001) and briefly centrifuged at 300 ×g prior to measuring fluorescence intensity (FI) using FLIPR (Fluorescent Imaging Plate Reader) with kinetic measurements taken every 10 seconds for 360 reads. Final assay concentrations of kinase 1, AQT-099, ATP and DMSO were 100nM, 10uM, 90µM and 1%, respectively.

1.2.4. FLIPR Tetra data acquisition system

The biochemical kinetic assay was monitored using the 384 FLIPR Tetra, a high-throughput kinetic screening system with a high sensitivity CCD camera capturing fluorescence intensity recordings in all 384 wells simultaneously. The incorporated SoftMax Pro software flexibility allows specific parameters to be chosen in the protocol to enhance assay performance and sensitivity. The assay was run using the following modified protocol: the fluorescent intensity was measured at 360 nm ± 20 nm excitation (Ex) / 545 nm ± 30 nm emission (Em), gain: 40, exposure time: 30 seconds, excitation settings: 80% with read time intervals every 10 secs for 360 reads. Following the completion of the run, substrate bias corrected data was automatically exported into an assigned folder configured in the Auto-Export settings.

1.2.5. Data Analysis

Preliminary visualization of progress curves was done using SoftMax software associated with FLIPR. Kinetic raw data was analyzed using the Genedata Kinetic Analyzer module. Neutral (100% activity) and inhibitor (0% activity) controls were used to assess signal window and assay linearity. To eliminate background noise, data was normalized by subtracting the average of inhibitor controls from the whole data set. Normalized data were used for progress curve analysis for computing k_{inact}/K_I^{app} (apparent k_{inact}/K_I). Automated data importation followed by fully interactive analysis significantly reduced the time required for data analysis contributing to the purpose of delivering a high-throughput system. For low-throughput analysis, GraphPad Prism version 8.1.2 was used.

1.2.6. Determination of k_{inact}, K_I, and k_{inact}/K_I from total progress curve analysis

The below depicted scheme represents both covalent irreversible inhibition and slow onset inhibition that results from either binding and covalent bond formation or from binding, isomerization and subsequent trapping of the inhibitor to the target site on the enzyme[7].

$$[E] + [I] \underset{k_{-1}}{\overset{k_1}{\rightleftharpoons}} [EI] \underset{k_{-2}}{\overset{k_2}{\rightleftharpoons}} [EI]^*$$

Where, E and I are free enzyme and inhibitor respectively, EI is the non-covalent complex between Enzyme and Inhibitor and EI^* is either the covalent complex or the isomerized complex where the inhibitor is trapped. The rate constant k_2 is equivalent to k_{inact} in the case of covalent irreversible inhibition. k_{-2} would be zero for all practical purposes for covalent irreversible inhibitors and extremely slow for slow-onset inhibitors[25][26]. For covalent inhibitor, K_I, inhibitor concentration at half maximal inhibition rate when all the inhibitor is complexed with enzyme, is defined as (k_{-1} +

k_2)/ k_1. This reduces to the equilibrium dissociation rate constant K_i (k_{-1}/ k_1) when the maximum rate of inactivation is extremely slow compared to the rate at which EI dissociates to E and I, respectively. Complete progress curves were generated and fit to Equation 1 for data generated using covalent inhibitors.

$$P = \left(\frac{V_i}{k_{obs}}\right)\left(1 - e^{-k_{obs}*t}\right) \ldots\ldots \text{Equation 1}$$

The k_{obs} estimated from this fit was plotted as a function of inhibitor concentration and the resultant data points were either fitted to a linear equation for one-step covalent inhibition or fitted to equation 2 for two-step covalent inhibition to extract k_{inact} and K_I.

$$k_{obs} = \frac{k_{inact}[I]}{[I] + K_I} \ldots\ldots\ldots \text{Equation 2}$$

Though covalent irreversible inhibition is most often a two-step process, oftentimes the curve of k_{obs} vs [I] appears linear for reasons that have been extensively discussed elsewhere[7]. Briefly,

$$\frac{k_{inact}}{K_I} = \frac{k_{inact}}{\frac{(k_{inact} + k_{off})}{k_{on}}} = \frac{k_{on} \times k_{inact}}{k_{inact} + k_{off}}$$

When the value of k_{inact} is far less than k_{off} (weak inactivation), the term can be ignored in the denominator and k_{inact}/K_I is equal to ($k_{on} \times k_{inact}$)/k_{off} (or k_{inact}/K_i). Under these conditions, the k_{obs} versus [I] plot would appear linear because achieving inhibitor concentration that would yield maximal inactivation, and thus the zero order phase of the curve, would be untenable. On the other extreme, when k_{inact} is far greater than k_{off} (both binding and inactivation are potent), the k_{off} term in the denominator can be ignored and that would make the k_{inact}/K_I term equal to k_{on}. In this latter case too, the k_{obs} versus [I] plot would appear linear because at high inhibitor there would be potent inhibition making it difficult to estimate the correct k_{obs} from fits to the data. Any case in between the above mentioned extremes would yield non-linear hyperbolic plots for the k_{obs} versus [I] plots. As mentioned earlier, when the plot appeared linear, the experimental data points were fit using linear regression with the slope of the line providing an estimate of the ratio between k_{inact} and K_I (k_{inact}/K_I)[27]. However, care has to be exercised to ensure that the inhibition is covalent and irreversible in nature (and not slow onset) using orthogonal measurements before applying this analysis.

1.3. Results

The main objective for an assay development effort is to standardize reaction conditions that can identify modulators of an enzyme's activity providing detailed insights into their mode of action vis-à-vis the target in a cost and time effective manner. A robust assay should show the traits of being sturdy, homogenous, linear, cost effective with a threshold expense per well that is well within the project's budget and is capable of handling the number of compounds that is aimed to be tested. Further, it should have a variability coefficient of less than 10 %, a signal/noise ratio above 8, should yield assay output within a reasonable window of time and should confer clearly quantifiable benefits over currently existing methodologies (Figure 1 A). The FLIPR tetra based assay reported here was developed using the above-mentioned guidelines for optimization of the reaction conditions and further implementation in a high-throughput format.

1.3.1. Assay Development: Often, biochemical assays providing kinetic information suffer from the disadvantages of not being compatible with high-throughput format. We have developed a FLIPR tetra

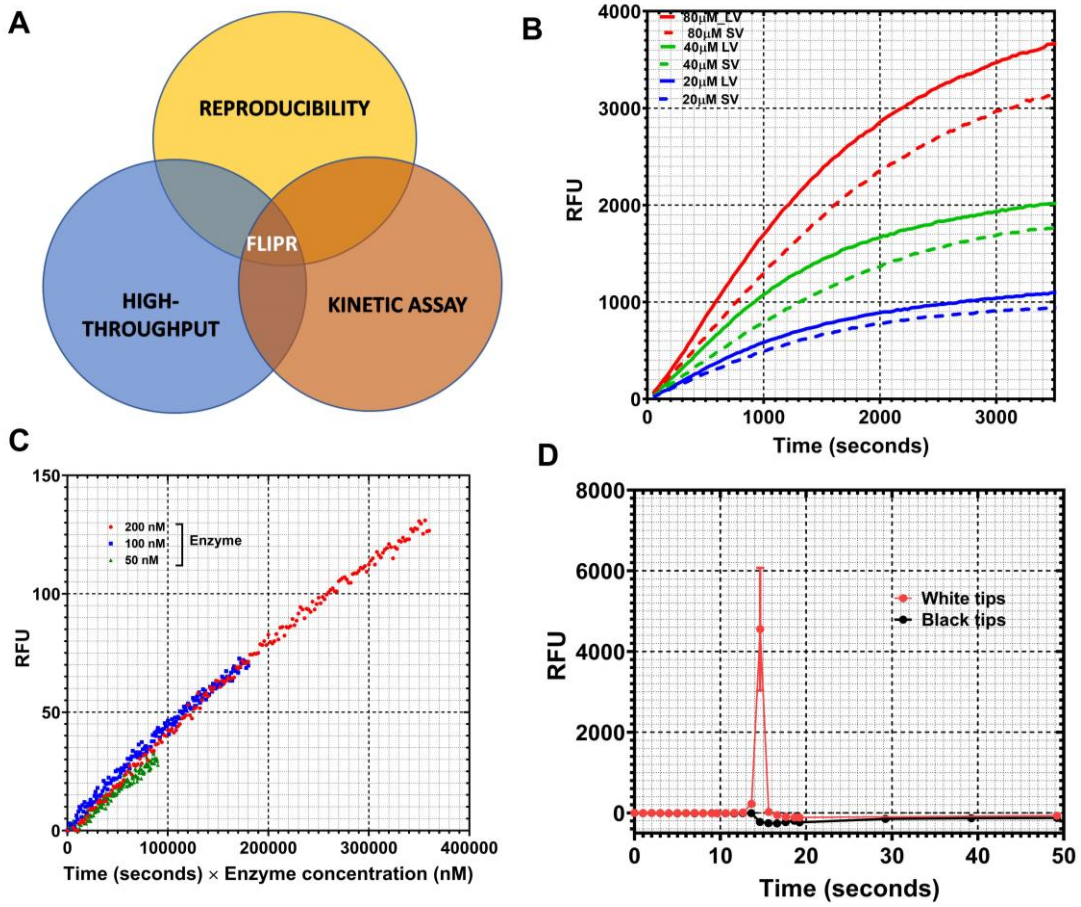

Figure 1. *Assay optimization for Structure-Kinetic data driven medicinal chemistry (A) A Venn -diagram illustrating the strengths that FLIPR based approach bring to routine profiling efforts (B) Optimization of low volume (LV) and high volume (SV) plates (C) Selwyn's test for understanding enzyme inactivation as a function of time and plate type in low-volume plates (D) Optimization of tip types to get rid of the spike signal considering the bottom up reading-mode of FLIPR tetra.*

based assay as a means to overcome the above stated limitation. FLIPR tetra is often used for high-throughput cellular screening. Though a couple of studies have implemented FDSS (Functional drug screening system) for biochemical assays in the HTS format[28], to the best of our knowledge, none have reported the application of FLIPR tetra for biochemical assays. However, most of them are point measurements with very insignificant, if any, kinetic aspect to them. The assay was standardized with the cytosolic domain of kinase target 2, a receptor protein tyrosine kinase. The assay development phase was aimed at optimization of several different parameters. Conventionally, high volume 384-well plates (100 µl maximum and 20 µl minimum volume) are employed in FLIPR for carrying out cellular assays. However, these volumes are incompatible with biochemical assay setup from the cost (monetary and reagent) perspective. Hence, optimization of the assay with low volume 384-well plates was undertaken and was geared towards making the assay compatible with high-throughput format to develop a generalized applicability for expensive reagents employed in biochemical assay settings. After initially assessing whether the biochemical assay yielded the necessary signal/noise using standard high volume plates, it was miniaturized to low volume plates (50 µl maximum volume) and the assay was run in a total volume of 10 µl. Figure 1B shows the progress curves for the high-volume and low-volume formats obtained with 10 nM of kinase-2 enzyme. As

can be seen, the signal intensity across the two different plate formats was comparable within experimental variation. In fact, the low-volume format showed slightly better signal/noise ratio compared to the high-volume format (Figure 1B).

Progressive inactivation of protein is an important parameter to be optimized in an assay optimization exercise. Often, the nature of the plate employed can have important implications for enzyme inactivation and, thus, assay stability. Selwyn's test[29] was carried out to assess whether there was any protein activity loss as a function of the newly implemented low-volume plate format. In this assessment, velocity is plotted as the product of time and enzyme concentration. Any evident non-linearity of the plots as a function of enzyme concentration variation would be indicative of protein inactivation. Figure 1C shows the outcome of Selwyn's test for kinase 1. As is evident from the figure, there is no significant non-linearity as a function of protein concentration variation for kinase 1 indicating that the protein does not lose activity as a function of time with low-volume plates.

Different tip types with specific coatings can have significant carry over (CO) effect and potential for assay interference and irreproducibility[30]. Given the low-volume nature of the FLIPR based assay, two different tip types were assessed for their effect on the assay outcome. Figure 1D shows the results for assay signal readout employing black and white tips, respectively. As is evident from the figure, white tips result in an artifactual spike in the signal while black tips do not show any spikes indicating minimal signal interference by the latter vis-à-vis the former. It is likely that the white tips interfere with the excitation source as they pipette into the reaction plate that is read through the bottom.

Most HTS exercises and kinetic characterization of inhibitor MoA studies are undertaken by dissolving the compounds in the aprotic solvent DMSO that is capable of dissolving both polar and apolar compounds. This is optimal given that pharmaceutical companies screen millions of different compounds during their initial HTS exercise and use of DMSO as the base solvent helps maintain invariability across the screen. This is irrespective of the fact that DMSO could act as an inhibitor of some enzymes[31]. It was observed that some reaction progress curves showed a blip when monitored in the presence of DMSO in the reaction mix (data not shown). The blip was observed at around 750 seconds after initiation of the reaction. However, it would have to be noted that the blip was not consistent and was independent of enzyme concentration in the reaction mix and was seen in the no enzyme background curve too. The blip was absent when the assay was carried out under identical conditions in the absence of DMSO (Figure 2A). Hence, it is surmised that the blip is possibly indicative of some DMSO-mediated effect. A DMSO-induced blip would be contra productive to a high-throughput screening or characterization exercise because of the reason specified above. Hence, several conditions were explored to get rid of the blip in the progress-curve measurements. It was observed that sealing the plate after initiation of the reaction leads to complete abolishment of the blip. Further, the seal helps in reducing the background signal associated with the substrate effectively as is shown in Figure 2B in the absence of DMSO and enzyme. This could be because of possible control on the rate of evaporation and due to the unique optics of the FLIPR-tetra assay setup.

Signal saturation is an essential parameter to optimize to ensure that the assay is carried out within reasonable window for reproducibility. Signal saturation is usually

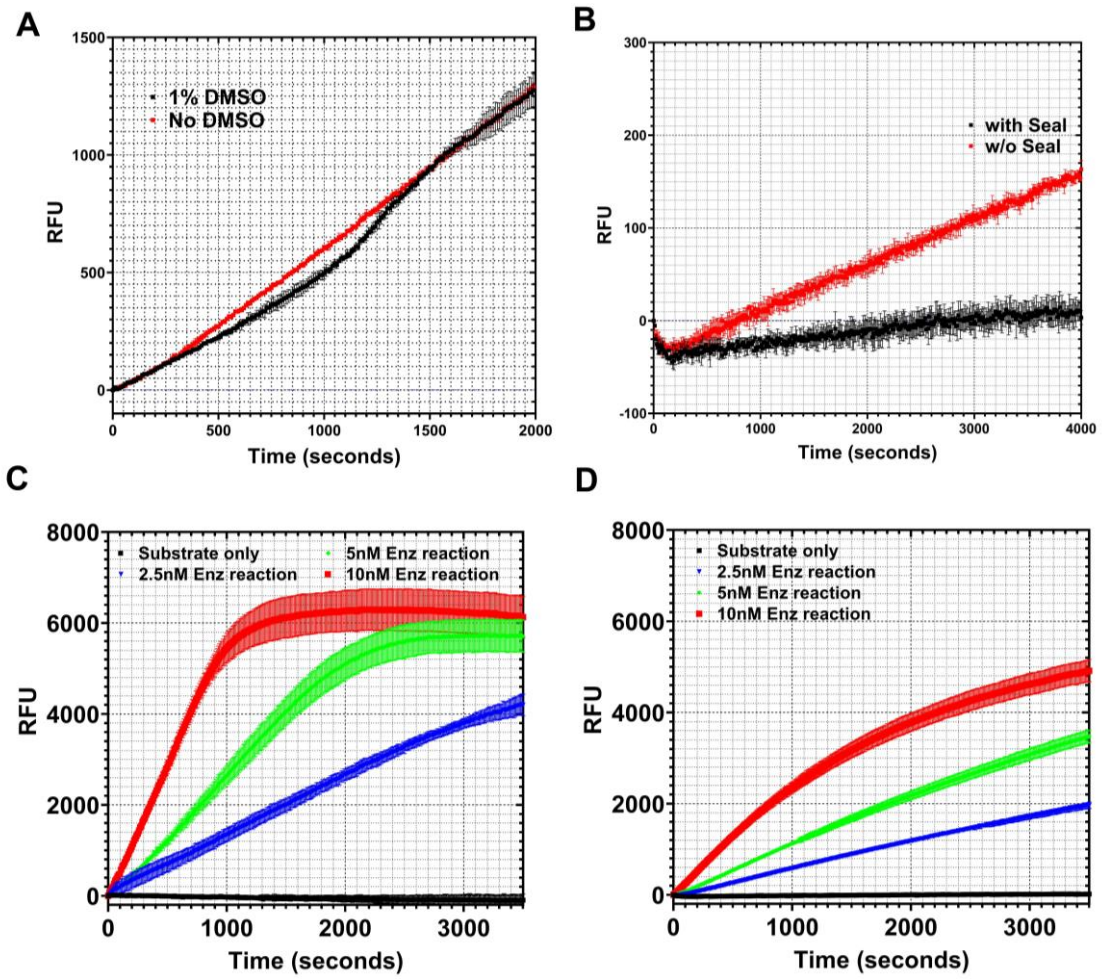

Figure 2. *Assay optimization for Structure-Kinetic data driven medicinal chemistry (A) DMSO mediated blip in progress curves. Inset shows that the DMSO mediated blip is enzyme independent. Sealing the plate gets rid of the blip. (B) Sealing the plate also helps with reduction of background signal as a function of time. (C) Data acquired at high excitation settings (50 Gain, 0.4 Exposure and 100 % intensity) (D) Data acquired at low excitation settings (50 Gain, 0.1 Exposure and 50 % intensity).*

very well defined and sharp in other readers (PheraStar and Envision). A unique feature of assay monitoring in FLIPR is the deviation from sharp signal saturation. In FLIPR, the signal saturation is very gradual and variable, starting its deviation from linearity above 4000 signal counts. Initial observation of non-linearity in reaction progress curves led the authors to suspect potential substrate depletion or product inhibition. However, the outcome from carrying out the assay under identical conditions at high excitation setting (50 Gain, 0.4 Exposure and 100 % intensity) and low excitation settings (50 Gain, 0.1 Exposure and 50 % intensity) at different concentrations of enzyme refuted the above suspicion (Figure 2C and 2D). As is seen in Figure 2D, the signal saturation vanishes indicating that the saturation is likely because of instrumental limitation rather than biological outcomes like substrate depletion or product inhibition. Therefore, it would be optimal to carry out the studies with a basal fluorescence signal of a minimum 1000 to maximum 2000 counts over the background signal that is way below the saturation bandwidth of the camera (6000 and 7000 counts for the AssayQuant peptides AQT0099).

Optimization efforts were validated with parallel investigation of the same dataset using conventional biochemical readers

(Photo multiplier tube readers-PMT) (data not shown).

1.3.2. Assessment of assay implementation in a target agnostic manner: assessment with various kinases

An assay development effort should invest considerable time and effort in demonstrating the generality of the setup in a target agnostic manner across several therapeutic functionalities. To demonstrate the generality of the FLIPR-based approach, as a first step, we employed it on several different kinases to generate biochemical kinetic data. Prominent distinct kinase targets anonymized as kinase 1, 2, 3 and 4 were assayed at various concentrations of their respective inhibitors with assay quant technology. Figure 3 shows the progress curves for the various kinases at several different inhibitor concentrations (Figure 3A, B, C and D). As is evident in the plots, the progress curves for the various enzymes are clearly indicative of non-linearity as is expected for either covalent irreversible, slow-binding inhibition or, occassionally, for covalent reversible inhibition. Other curves are linear as expected for equilibrium reversible inhibitors. Further, these results show that the FLIPR platform can be used in a target agnostic manner to generate SKR data for multiple kinases.

1.3.3.Low-throughput kinetic parameter estimation from full progress curve analysis and need of confluent datapoints for accurate parameter estimation

Low-throughput kinetic parameter estimation was performed using methods indicated in materials and methods. The reaction progress curves at several different concentration of the inhibitors were fit using equation 1 to extract the parameter k_{obs} that provides a measure for the rate of transition from the initial velocity to the steady-state velocity as a function of time-dependent inhibition shown by covalent or slow-onset inhibitors. For the former case, the steady state velocity can be constrained to zero while in the latter it is >0 but $<v_i$. The k_{obs} values were plotted as a function of inhibitor concentration and the resultant experimental data points were fit using linear regression and equation 2 simultaneously to see whether they either conform to the one-step model or the two step model, respectively, when assessing covalent inhibitors. Appropriate model selection was made based on model comparison using statistical tests like non-nested Akaike's Information Criterion (AIC) or nested extra sum-of-squares F-test. Depending on the model, we either obtain k_{inact}/K_I as a composite term (slope of the line) for one-step model or individually resolved values of k_{inact} and K_I for two-step model. The resolution helps in guiding the chemists with individual optimization of both chemical reactivity of the warhead and the apparent binding magnitude embedded in the K_I term for the covalent inhibitor or lead molecule. The experimental data showed that there was time-dependent loss in reaction velocity in addition to the concentration dependence of inhibition (Figure 4A top panel). Further, it is also clear that some curves showed the two-step binding that is typically expected with covalent inhibitors having a distinct binding step and a reactivity step while others show a one-step behaviour likely because (1) the reactivity step is a lot faster than binding, (2) at high-inhibitor concentrations the progress curves are noisy precluding reliable slope estimations and/or (3) the binding is non-specific and is modifying more than one group on the enzyme. Possibility number (3) is unlikely given the care with which these inhibitors are designed and the fact that there is a single cysteine nucleophile on the kinase target that is targeted by the prosthetic group confering binding. As a comparative case-study, we also show the linear progress curves for compounds having extremely slow k_{on} rates or those that show reversible binding.

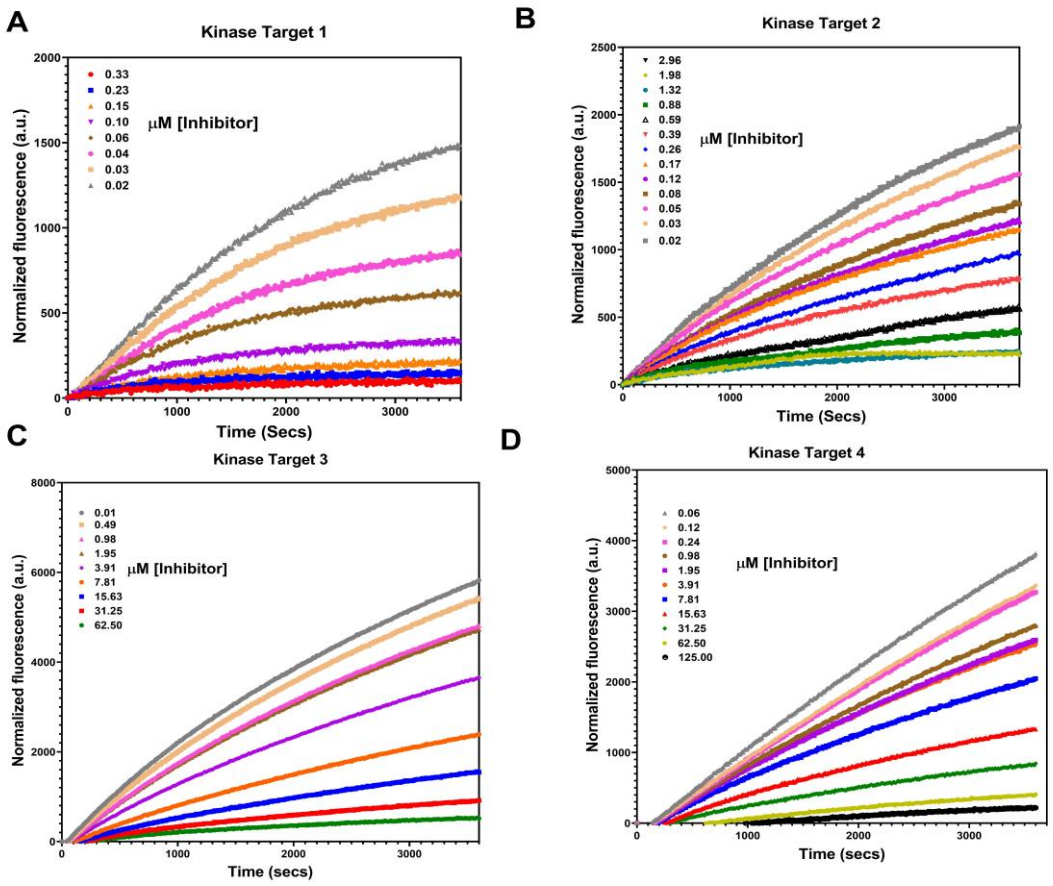

Figure 3. *Assessment of FLIPR tetra based assay as a target agnostic platform for several different targets (A) Kinase 1 (B) Kinase 2 (C) Kinase 3 (D) kinase 4.*

A typical progress curve for an inhibitor comprises a quantitative measure of enzyme activity plotted against time at continuously varying concentration of inhibitor. The quality of the progress curve and analyzed data improves by the reducing time intervals of kinetic reads. Standard PMT based plate readers read one well at a time and therefore for reading a full 384-well plate, the shortest time interval is usually ~1.5 min in "precise" laser mode, which is unacceptably large. Likewise, a full 1536 plate would be read in roughly 6 minutes on standard PMT readers for "precise mode". Though other modes like "rapid" and "flying" mode can reduce the time, the quatum yield can get dramatically effected because of reducing number of flashes. Using standard PMT-based plate readers, only three rows of a 384-well plate was read continuously to reduce time intervals to ~30 seconds per read. A maximum of 4 compounds (16-points) could be accommodated in three rows of 384-well plate limiting the throughput of biochemical kinetic assays. In contrast, the CCD camera within FLIPR captures whole-plate level data per read which allows reducing the time interval to as low as 1 second per read irrespective of the plate type, 384 or 1536. FLIPRs have been used extensively for cell-based assays for many years but their application to biochemical kinetic assays for determination of mechanistic parameters like k_{inact}/K_I has never been reported. The current study validated FLIPR for 384-plate based biochemical kinetic assays based on AssayQuant technology. The FLIPR method reads whole plates comprising 18 compounds every 10 seconds whereas standard PMT readers could not accommodate more than one compound (16-points) in 10 second time interval. Therefore

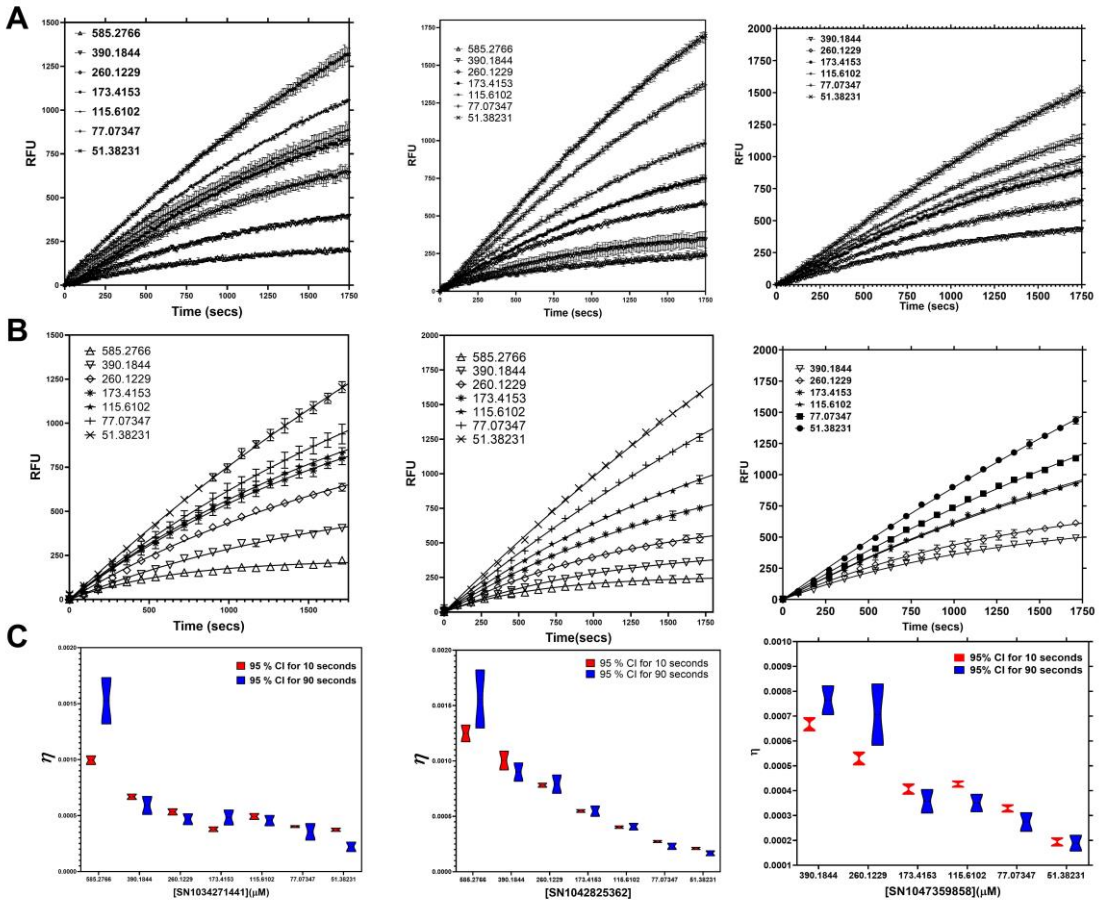

Figure 4. *The contribution of data confluency to parameter estimation (A) Data acquired with 10 seconds confluency and fitted globally to the model for irreversible covalent inhibition for three distinct compounds (B) Data acquired with 90 seconds confluency and fitted globally to the model for irreversible covalent inhibition for three distinct compounds (C) plot of 95 % confidence interval spread for a parameter (η) as a function of compound concentration for the three compounds assessed above at 10 seconds and 90 seconds confluency.*

an 18-fold increase in throughput is achieved using FLIPR as a reader.

Covalent compounds and compounds with slow onset of binding usually show non-linear progress curves distinguishing the binding step from inactivation/conformational reordering steps, respectively. The confluence of data points at the zone of transition determines, to a large extent, the validity of k_{obs} and, subsequently, k_{on}^{app} and k_{off} derived from secondary replots. With this knowledge, we attempted assessing the data obtained from FLIPR Tetra at two different time-intervals. The analysis was performed for 3 different compounds at 14 concentrations each. The time-course measurements were carried out with four technical replicates at 10 seconds and 90 seconds confluence, respectively. Compound concentrations yielding zero activity as a function of time were eliminated for reliable global fits. The time-course data points were fit to equation (1) for non-linearity as a result of inhibition for both the 10 seconds and the 90 seconds confluency data (Figure 4A and 4B). The resultant plot of 95 % confidence interval (C.I.) of the parameter from the fits for the 90 second and 10 second confluence data are shown in Figure 4C bottom panel. As is evident from the figure, the confluence of data points plays a major role in the accuracy of parameter estimation. The 95 % C.I. of the η parameter obtained from fits are broader for data collected at 90 seconds than that collected at 10 seconds confluence. Further,

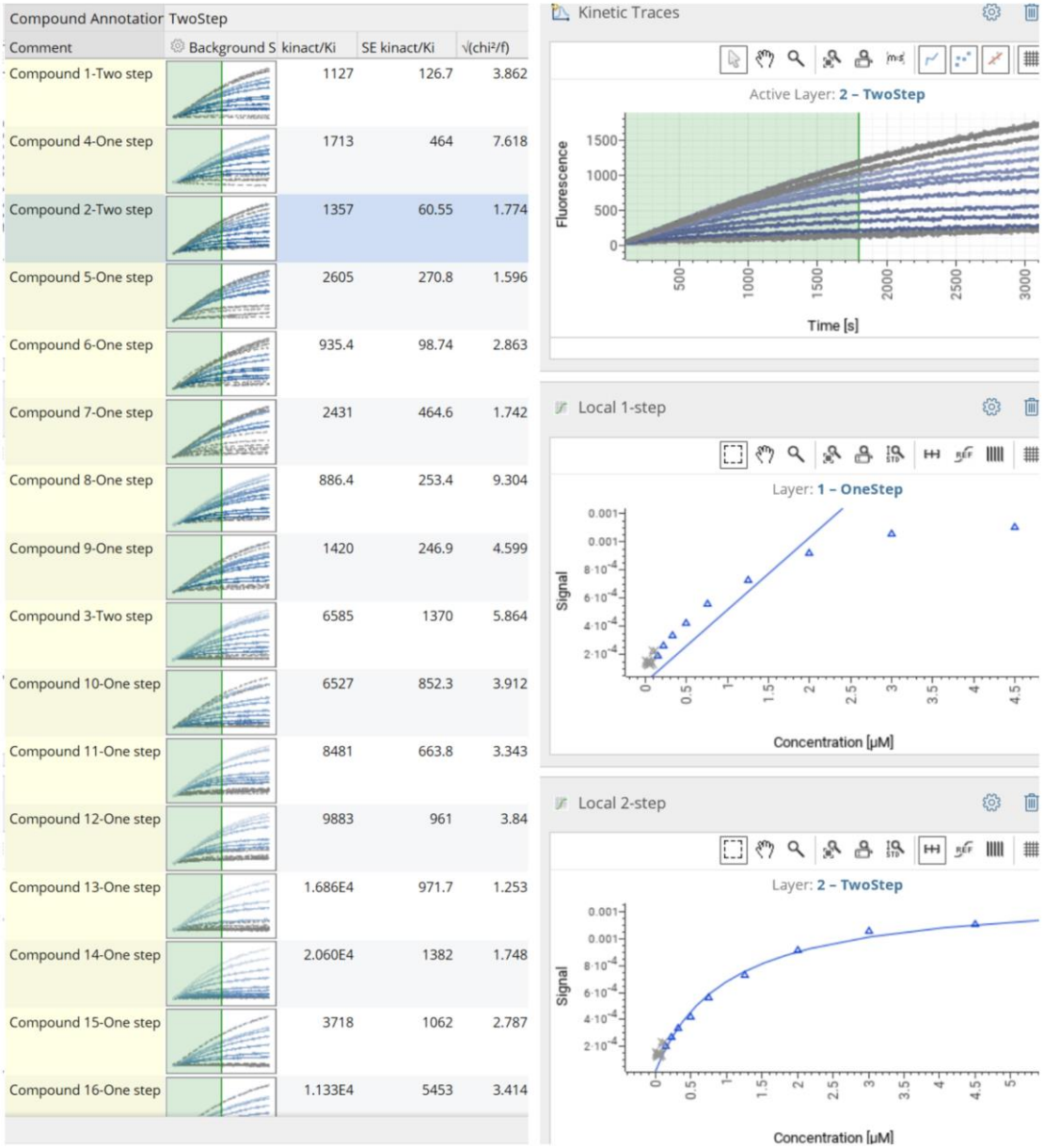

Figure 5. *A snapshot of the gene data session showing high-throughput analysis of the data generated by FLIPR. The left panel shows the progress-curves of the enzyme's conversion of substrate to product as a function of varying inhibitor concentrations. The right panel indicates secondary replots of the kobs as a function of inhibitor concentration to discriminate between one-step and two-step binding.*

as is evident from the trend of η variation as a function of inhibitor concentration, the mean estimate of the parameters itself is offset when the data is collected at 90 seconds time interval. This aspect emphasizes the importance of using FLIPR tetra to acquire confluent data points in estimating reliable parameters from kinetic runs.

1.3.3.High-throughput data analysis and reporting in the Genedata package

Raw data SEQ. files were automatically exported from FLIPR in a fixed format compatible with a FLIPR Genedata kinetic parser. Data files were imported into a predefined Genedata template for calculating k_{inact}/K_I values of covalent inhibitors of kinase target 1. Data quality was assessed using signal intensity, linearity and variability of progress curves from both positive controls (100 % activity) and negative controls (100 % inhibition). Data

was normalized for background noise by subtracting average of negative controls from whole data set. The template is defined with equations for both one-step and two-step binding which calculates observed rate constant (k_{obs}) for all sixteen concentrations (10 µM-0.0175 µM) of a particular inhibitor. As a standard practice, k_{obs} values for progress curves showing full/no inhibition were invalidated. The shape of k_{obs} vs [Inhibitor] was visually examined to decide one-step or two-step binding. However, efforts are ongoing to remove the subjectivity of this analysis by instituting appropriate statistical parameters to assess the curves such as AIC or F-test based assessments as indicated elsewhere in the manuscript. Linear correlation confirmed one-step binding while hyperbolic correlation was decided as two-step binding.

Figure 5 shows a screenshot of visualization from a standard Genedata analysis session. On the top right, plot named "Kinetic Traces" shows visualization of progress curves for a 16-point serial dilution of a tested inhibitor compound named as "Compound 2". Concentration-dependent reduction in signal intensity is evident without any noticeable increase in noise. Plots named "Local 1-step" and "Local 2-step" shows k_{obs} for all progress curves for Compound 2 against inhibitor concentration, fitting to the one-step model and two-step models, respectively. In this case Compound 2 showed a two-step binding behavior as confirmed by a hyperbolic fit in the "Local 2-step" plot, and therefore corresponding k_{inact}/K_I value was reported. Likewise k_{inact}/K_I values of all 18 tested inhibitors preferring either the one-step or two-step model was determined.

Assay reproducibility was investigated by comparing k_{inact}/K_I from three independent occasions, as enlisted in Table 1 along with mean ± SEM values. Low standard errors across a broad range of k_{inact}/K_I values (50 $M^{-1}S^{-1}$ to 15000 $M^{-1}S^{-1}$) confirmed excellent assay reproductivity.

1.3. Discussion:

Assays are a vital part of biomedical research. Design, assembly and execution of an assay that is sturdy, sensitive and capable of detecting a specific metabolite accurately plays an important part in the modern drug discovery process[32]. It is pivotal that, apart from the core aspects of the assay, a systematic workplan is instituted that takes into consideration aspects such as sample preparation and the data analysis pipeline. Moreover, a strong balance would have to be achieved between data fidelity and the high-throughput nature of the assay. Here we have specifically implemented FLIPR as a platform to perform high-hroughput kinetic assays. FLIPR was initially developed with an aim to carry out quantitative screening for cell-based kinetic assays[33–35]. The unique aspect of FLIPR that has been exploited extensively in the current work is that all the wells of a standard microplate are primed and optically measured simultaneously. Data from all the wells can be obtained in under 1 second, allowing for transient signals to be quantified. This feature is an absolute must for carrying out kinetic studies requiring the acquisition of highly confluent data points in a time-dependent manner. FLIPR has been used in applications such as estimation of intracellular calcium concentrations, GPCR and ion-channel activity, changes in intracellular pH and membrane potential[36–38].

There is an increased appreciation for incorporating biochemical kinetic data in early drug discovery. This is done with the intent of integrating BK of the drug with its pharmacokinetics and pharmacodynamics to get a unified perspective on how the drug molecule navigated through its ingestion, incorporation, interaction and clearance (I^3C) cycle to bring about the desirable therapeutic outcome. This has been

exemplified by increased research thrust within the pharmaceutical industry in achieving this objective and efforts at establishing academia-industry incubators to accelerate the innovation of new toolkits for its speedy realization. A prominent example is the Kinetics for Drug Discovery (K4DD) consortium funded by Innovative Medicines initiative (IMI) in partnership with major pharmaceutical companies[20].

An appreciation for the kinetics of target inhibitor interaction would inform the rational optimization of leads as drugs. This is exemplified by two relevant case studies below. Let us assume a case where the clearance (pharmacokinetics) of the drug from the system is rapid while sustained target engagement is a desirable trait for disease amelioration or dosing decisions. A program optimizing for drug residence time (very slow k_{off} rates) would essentially decouple pharmacodynamics from pharmacokinetics resulting in longer residence time ($1/k_{off}$) of the drug on the target (conferring the needed therapeutic modality) and thus, optimal and desirable pharmacological benefits. A prominent example of this is the drug desloratidine. Desloratidine is a Histamine H1 receptor antagonist that is approved for the treatment of Hayfever. The beneficial effect of desloratidine is because of its long residence time (190 ± 40 min)[39]. The second case study is of drug molecules that show target interaction mediated toxicity. In this case, optimizing for a drug molecules with fast on and off rates, respectively, would yield the desirable benefit of reducing toxicity and faster clearance. An example of the above modality is Quetiapine. The drug is an antagonist for the Dopamine D2 receptor that is administered for treating schizophrenia and bipolar disorders. An extremely slow k_{off} rate, leading to prolonged drug target residence-time, can lead to undesirable clinical outcomes of drug administration revealed as movement disorders (muscle contraction, spasms and so forth). In retrospect, it is known that Quetiapine is a successful drug to treat this condition because of its reasonably fast k_{off} rates that prevents the undesirable side-effects while being an effective cure for blocking D2 receptors. Hence, knowledge on, and incorporation of, structure kinetic relationship between a small-molecule and its target's interaction is an absolute requirement for success of a small-molecule therapeutic modality in a clinical indication-oriented manner.

Summary: In summary, we have increased the quality and confluence of high-throughput kinetic data by using FLIPR as a reader. We validated that CCD based camera technology could be one of the ways forward for capturing fast biochemical kinetics where laser-based plate readers usually struggle. The next step for us would be optimizing 1536-well plate reads on FLIPR for a biochemical kinetic assay that would further increase throughput from 18 compounds to 72 compounds per run. Also, our future attempts would be to utilize "simultaneous pipette and read" capability within FLIPR.

Acknowledgements: We would like to acknowledge Rachel Grimley, Geoff Holdgate, James Robinson, Paul Helmsley, Argyrides Argyrou, Ray Finley, Dynes Therese, Gavin Collie, Michaelides Iacovos, Anne Jackson, Xiang Zhai and Omar Alkhatib for their help during this work and/or for their critical inputs on the manuscript that enabled its improvement.

Conflict-of-interest: The author declares no conflict of interest.

References

[1] M. Vilums, A. J. M. Zweemer, Z. Yu, H. De Vries, J. M. Hillger, H. Wapenaar, I. A. E. Bollen, F. Barmare, R. Gross, J. Clemens, P. Krenitsky, J. Brussee, D. Stamos, J.

Saunders, L. H. Heitman, A. P. Ijzerman, *J. Med. Chem.* **2013**, *56*, 7706–7714.

[2] Z. Yu, J. P. D. Van Veldhoven, J. Louvel, I. M. E. 'T Hart, M. B. Rook, M. A. G. Van Der Heyden, L. H. Heitman, A. P. IJzerman, *J. Med. Chem.* **2015**, *58*, 5916–5929.

[3] H. Lu, J. N. Iuliano, P. J. Tonge, *Curr. Opin. Chem. Biol.* **2018**, *44*, 101–109.

[4] F. Schiele, P. Ayaz, A. Fernández-Montalván, *Anal. Biochem.* **2015**, *468*, 42–49.

[5] B. Srinivasan, *FEBS J.* **2020**, DOI 10.1111/febs.15537.

[6] G. Dahl, T. Akerud, *Drug Discov. Today* **2013**, DOI 10.1016/j.drudis.2013.02.010.

[7] R. A. Copeland, *Evaluation of Enzyme Inhibitors in Drug Discovery: A Guide for Medicinal Chemists and Pharmacologists: Second Edition*, **2013**.

[8] R. A. Copeland, D. L. Pompliano, T. D. Meek, *Nat. Rev. Drug Discov.* **2006**, DOI 10.1038/nrd2082.

[9] R. A. Copeland, *Expert Opin. Drug Discov.* **2010**, DOI 10.1517/17460441003677725.

[10] W. E. A. de Witte, M. Danhof, P. H. van der Graaf, E. C. M. de Lange, *Trends Pharmacol. Sci.* **2016**, DOI 10.1016/j.tips.2016.06.008.

[11] W. E. A. de Witte, M. Danhof, P. H. van der Graaf, E. C. M. de Lange, *Nat. Rev. Drug Discov.* **2018**, DOI 10.1038/nrd.2018.234.

[12] K. S. S. Lee, J. Yang, J. Niu, C. J. Ng, K. M. Wagner, H. Dong, S. D. Kodani, D. Wan, C. Morisseau, B. D. Hammock, *ACS Cent. Sci.* **2019**, DOI 10.1021/acscentsci.9b00770.

[13] G. M. Keserü, D. C. Swinney, *Thermodynamics and Kinetics of Drug Binding*, **2015**.

[14] D. A. Schuetz, W. E. A. de Witte, Y. C. Wong, B. Knasmueller, L. Richter, D. B. Kokh, S. K. Sadiq, R. Bosma, I. Nederpelt, L. H. Heitman, E. Segala, M. Amaral, D. Guo, D. Andres, V. Georgi, L. A. Stoddart, S. Hill, R. M. Cooke, C. De Graaf, R. Leurs, M. Frech, R. C. Wade, E. C. M. de Lange, A. P. IJzerman, A. Müller-Fahrnow, G. F. Ecker, *Drug Discov. Today* **2017**, DOI 10.1016/j.drudis.2017.02.002.

[15] P. J. Tonge, *ACS Chem. Neurosci.* **2018**, *9*, 29–39.

[16] A. C. Pan, D. W. Borhani, R. O. Dror, D. E. Shaw, *Drug Discov. Today* **2013**, DOI 10.1016/j.drudis.2013.02.007.

[17] S. J. Teague, *Nat. Rev. Drug Discov.* **2003**, DOI 10.1038/nrd1129.

[18] N. Ferruz, G. De Fabritiis, *Mol. Inform.* **2016**, *35*, 216–226.

[19] J. M. Strelow, *J. Biomol. Screen.* **2017**, *22*, 3–20.

[20] D. Guo, L. H. Heitman, A. P. Ijzerman, *ChemMedChem* **2015**, *10*, 1793–1796.

[21] M. D. Shults, B. Imperiali, *J. Am. Chem. Soc.* **2003**, DOI 10.1021/ja0380502.

[22] L. B. Peterson, B. Imperiali, in *Concepts Case Stud. Chem. Biol.*, **2014**, pp. 1–16.

[23] M. D. Shults, K. A. Janes, D. A. Lauffenburger, B. Imperiali, *Nat. Methods* **2005**, DOI 10.1038/nmeth747.

[24] M. D. Shults, D. Carrico-Moniz, B. Imperiali, *Anal. Biochem.* **2006**, DOI 10.1016/j.ab.2006.03.003.

[25] B. Srinivasan, **2020**, DOI 10.20944/preprints202010.0179.v1.

[26] B. Srinivasan, J. Skolnick, *FEBS J.* **2015**, *282*, 1922–1938.

[27] X. Zhai, R. A. Ward, P. Doig, A.

Argyrou, *Biochemistry* **2020**, *59*, 1428–1441.

[28] E. VanderPorten, L. Frick, R. Turincio, P. Thana, W. LaMarr, Y. Liu, *Anal. Biochem.* **2013**, DOI 10.1016/j.ab.2013.07.003.

[29] M. J. Selwyn, *Biochim. Biophys. Acta* **1965**, *105*, 193–195.

[30] R. Weibel, M. Iten, I. König, R. Beckbissinger, T. Benthien, W. Hälg, N. Ingenhoven, A. Lehnert, L. Oeltjen, C. Zaborosch, *J. Lab. Autom.* **2010**, *15*, 369–378.

[31] L. Misuri, M. Cappiello, F. Balestri, R. Moschini, V. Barracco, U. Mura, A. Del-Corso, *J. Enzyme Inhib. Med. Chem.* **2017**, *32*, 1152–1158.

[32] B. Srinivasan, V. Kantae, J. Robinson, *Med. Res. Rev.* **2020**, DOI 10.1002/med.21670.

[33] K. S. Schroeder, B. D. Neagle, *J. Biomol. Screen.* **1996**, *1*, 75–80.

[34] D. F. Baxter, M. Kirk, A. F. Garcia, A. Raimondi, M. H. Holmqvist, K. K. Flint, D. Bojanic, P. S. Distefano, R. Curtis, Y. Xie, *J. Biomol. Screen.* **2002**, *7*, 79–85.

[35] K. L. Whiteaker, J. P. Sullivan, M. Gopalakrishnan, *Curr. Protoc. Pharmacol.* **2000**, *9*, 9.2.1-9.2.23.

[36] M. R. Arkin, P. R. Connor, R. Emkey, K. E. Garbison, B. A. Heinz, T. R. Wiernicki, P. A. Johnston, R. A. Kandasamy, N. B. Rankl, S. Sittampalam, *FLIPR™ Assays for GPCR and Ion Channel Targets*, **2004**.

[37] I. Vetter, *Adv. Exp. Med. Biol.* **2012**, *740*, 45–82.

[38] K. B. Hansen, H. Bräuner-Osborne, *Methods Mol. Biol.* **2009**, *552*, 269–278.

[39] R. Bosma, Z. Wang, A. J. Kooistra, N. Bushby, S. Kuhne, J. Van Den Bor, M. J. Waring, C. De Graaf, I. J. De Esch, H. F. Vischer, R. J. Sheppard, M. Wijtmans, R. Leurs, *J. Med. Chem.* **2019**, *62*, 6630–6644.

Table 1. Table of k_{ianct}/K_I from quadruplicate biological tests to establish the reproducibility of FLIPR tetra based assay format.

Compound ID	$k_{inact}/K_I(M^{-1}s^{-1})$ n=1	$k_{inact}/K_I(M^{-1}s^{-1})$ n=2	$k_{inact}/K_I(M^{-1}s^{-1})$ n=3	$k_{inact}/K_I(M^{-1}s^{-1})$ n=4	Std dev	Std error	Arithmetic Mean	Geomean
Compound A	10330	7885	10930	10310	1147.9	287.0	7131.3	9434.5
Compound B	9265	13180	13130	15220	2471.0	617.7	9416.3	12294.9
Compound C	8428	5974	8731	7632	1022.2	255.6	5508.5	7270.1
Compound D	5611	5667	8283	8579	1386.1	346.5	4964.3	6485.5
Compound E	3188	2455	4246	4981	1061.1	265.3	2656.0	3390.7
Compound F	1727	1233	1875	1994	315.3	78.8	1238.5	1619.3
Compound G	1603	1320	2622	2433	472.3	118.1	1339.0	1726.7
Compound H	1390	1945	1141	1122	342.7	85.7	1114.3	1447.6
Compound I	1040	885.2	1058	1355	195.5	48.9	820.1	1076.5
Compound J	588.2	472.2	715	639.2	69.9	17.5	424.9	562.0
Compound K	551.9	573.1	632.3	690.3	60.9	15.2	453.8	602.2
Compound L	328	203.8	504.2	415.5	86.9	21.7	236.8	302.8
Compound M	223.7	157.1	277.8	355.3	82.4	20.6	184.0	232.0
Compound N	169.7	180.1	331.3	338.2	77.1	19.3	172.0	217.8
Compound O	96.8	86.93	105.3	108.5	8.8	2.2	73.1	97.0
Compound P	123.7	617.2	446.7		161.5	53.8	190.1	235.1
Compound Q	1255	838.2	765.1		245.0	81.7	673.4	979.9
Compound R	2076	4396	4451		1187.5	395.8	2175.7	3039.8
Compound S	84.4	101.8			8.7	4.4	93.1	92.7